15th World Congress on Computational Mechanics (WCCM-XV)
8th Asian Pacific Congress on Computational Mechanics (APCOM-VIII)
Virtual Congress: 31 July – 5 August 2022
S. Koshizuka (Ed.)

REDUCED ORDER MODELING FOR MODULAR ANISOTROPIC STRUCTURES BASED ON PROPER ORTHOGONAL DECOMPOSITION AND MESH TYING

S. RITZERT[1], D. MACEK[1], J. W. SIMON[1] AND S. REESE[1]

[1] Institute of Applied Mechanics (IFAM)
RWTH Aachen University
Mies-van-der-Rohe-Str. 1, D-52074 Aachen, Germany
ritzert@ifam.rwth-aachen.de and https://www.ifam.rwth-aachen.de

Key words: Proper Orthogonal Decomposition, Mesh Tying, Anisotropy, Interpolation

Abstract. *A model order reduction technique in combination with mesh tying is used to efficiently simulate a large number of different structures that are assembled from a set of substructures. The stiffness matrices of the substructures are computed separately and assembled into a global stiffness matrix with tied contact formulation. The computational time can be further decreased by reducing the degrees of freedom of each substructure with a projection-based model order reduction technique. The precomputations to obtain the mode matrices are computationally cheap because they can be carried out on each substructure separately. For the development and optimization of new construction strategies for fiber reinforced concrete, a large number of different combinations of the modules have to be tested. The nonlinear anisotropic material behavior, like the primary directions of orthotropic materials, leads to parameter-dependent mode matrices. The precomputations can only be done for a relatively small number of parameters. For all other parameters, the mode matrices have to be adapted with interpolation methods to obtain an accurate solution .*

1 INTRODUCTION

A set of modules can be used to assemble different global structures. The mechanical analysis of these structures is computationally expensive. Model order reduction (MOR) techniques can be used to reduce the computational effort by projecting the equations into a lower-dimensional subspace [3] [5]. In this work, a MOR technique based on proper orthogonal decomposition (POD) is used [11]. In the past, the POD method has been applied to nonlinear solid mechanics [10] [14] [15]. We combine the MOR of modules with a tied contact formulation [17]. The stiffness and contact matrices of each module are projected into the reduced space individually. The global system of equations is then assembled from these reduced modules. The boundary and contact conditions can be chosen at will and depend on the assembled global system. In widely used component mode synthesis (CMS) methods like the Craig-Bampton method internal and interface degrees of freedom (DOF) are distinguished and only the internal DOFs are reduced. An overview of substructuring in structural dynamics is given in[7].

In this article, we focus on the directional material behavior of fiber-reinforced materials [16], which leads to parameter-dependent projection and stiffness matrices. These matrices are adapted to any fiber orientation by interpolation methods. The interpolation of projection matrices requires interpolation on a tangent space of the Grassmann manifold, which was first applied to reduced-order modeling in [2]. In [8] the stability of Grassmann interpolations is discussed in the context of parametric MOR

of mechanical problems with transversely isotropic materials. This interpolation falls into the class of manifold interpolations, where a general framework of Riemannian computation on manifolds was shown by Pennec et al. [12]. An overview of parametric MOR is given in [4]. The interpolation of the reduced system matrices as it is shown in [1] can not be applied in this work because the boundary conditions are not known beforehand and the projection matrices contain rigid body motions. Therefore, whole stiffness matrices have to be interpolated. In [9] stiffness matrices are approximated with a Taylor series expansion. In this work, the singular value decomposition (SVD) is used to reduce the high-dimensional interpolation to a sum of one-dimensional cubic spline interpolations.

2 REDUCED ORDER MODEL OF SOLID MECHANICS WITH TIED CONTACT

To describe modular systems mechanically, each substructure is described by the balance of linear momentum with additional contact conditions between different substructures. The balance of linear momentum of a substructure s in reference configuration reads

$$\begin{aligned} \operatorname{div}(\boldsymbol{F}^s\boldsymbol{S}^s)+\rho_0^s(\boldsymbol{b}^s-\ddot{\boldsymbol{u}}^s)=0 \qquad & \text{in } \Omega_0^s, \\ \boldsymbol{u}^s=\bar{\boldsymbol{u}}^s \qquad & \text{on } \Gamma_u^s, \\ \boldsymbol{F}^s\boldsymbol{S}^s\cdot\boldsymbol{N}^s=\bar{\boldsymbol{t}}_0^s \qquad & \text{on } \Gamma_\sigma^s, \end{aligned} \tag{1}$$

where $\boldsymbol{S}$ is the second Piola-Kirchhoff stress tensor, $\boldsymbol{F}$ the deformation gradient, ρ_0 the density in the reference configuration, $\boldsymbol{b}$ the body force and $\ddot{\boldsymbol{u}}$ the acceleration vector. Additionally the tied contact constraint

$$\boldsymbol{u}^s=\boldsymbol{u}^r \qquad \text{on } \Gamma_c^{s,r}, \quad \text{with } s\neq r, \tag{2}$$

has to be fulfilled. It states that the displacements $\boldsymbol{u}$ of two bodies on their contact interface Γ_c are equal. In the following, only quasi-static processes are considered, such that the acceleration vector $\ddot{\boldsymbol{u}}$ is neglected. The weak form of the above problem reads

$$g=\sum_{s=1}^{n_s}(g_{BLM}^s-g_c^s)=0, \tag{3}$$

where additional to the weak form of the balance of linear momentum g_{BLM} a contact term g_c has to be considered for every substructure. This contact can be interpreted as the virtual work done by the tractions $\boldsymbol{t}$ acting on the contact interface. The weak forms read

$$g_{BLM}^s=\int_{\Omega_0^s}(\boldsymbol{S}^s:\,\delta\boldsymbol{E}^s-\rho_0^s\boldsymbol{b}^s\cdot\delta\boldsymbol{u}^s)\mathrm{d}V-\int_{\Gamma_0^s}\bar{\boldsymbol{t}}_0^s\cdot\delta\boldsymbol{u}^\mathrm{d}A, \tag{4}$$

$$g_c^s=\int_{\Gamma_c^s}(\delta\boldsymbol{u}^s)^T\cdot\boldsymbol{t}^s\mathrm{d}A. \tag{5}$$

Considering two neighboring substructures, the forces on both sides of the contact surface have to be in equilibrium, which leads to the relation $\boldsymbol{t}^2=-\boldsymbol{t}^1$. This can be used to write the contact term as

$$g_c^1+g_c^2=\int_{\Gamma_c^{1,2}}((\delta\boldsymbol{u}^1)^T-(\delta\boldsymbol{u}^2)^T)\boldsymbol{t}^1\mathrm{d}A. \tag{6}$$

The tied contact constrained is enforced with a penalty parameter ε. With the definitions $\boldsymbol{w}^1:=\boldsymbol{u}_c^1-\boldsymbol{u}_c^2$, $\delta\boldsymbol{w}^1:=\delta\boldsymbol{u}^1-\delta\boldsymbol{u}^2$, and $\boldsymbol{t}^1:=\varepsilon\boldsymbol{w}^1$, the contact term is rewritten in a way hat can be discretized by finite elements

$$g_c^1 + g_c^2 = \int_{\Gamma_c^{1,2}} \delta \boldsymbol{w}^1 \varepsilon \boldsymbol{w}^1 \mathrm{d}A. \tag{7}$$

The finite element discretization of the weak form leads to the nonlinear system of equations

$$\sum_{s=1}^{n_s} \boldsymbol{R}^s(\boldsymbol{U}^s(t)) + \boldsymbol{K}_c^s \boldsymbol{U}^s(t) = \sum_{s=1}^{n_s} \boldsymbol{P}^s(\boldsymbol{U}^s(t)), \tag{8}$$

where $\boldsymbol{R}(\boldsymbol{U}(t))$ and $\boldsymbol{P}(\boldsymbol{U}(t))$ are the internal and external force vector respectively. The contact part of the equations is linear and contained in the matrix $\boldsymbol{K}_c$. For further information about tied contact finite element formulations the reader is kindly referred to [13].

In this model order reduction technique each substructure is reduced individually by a projection matrix $\boldsymbol{\Psi}_s$. The n-dimensional displacement vector $\boldsymbol{U}^s$ of a substructure s is approximated by a m-dimensional reduced displacement vector $\boldsymbol{U}^s_{\mathrm{red}}$ with

$$\boldsymbol{U}^s \approx \boldsymbol{\Psi}^s \boldsymbol{U}^s_{\mathrm{red}}. \tag{9}$$

The m columns of the projection matrix $\boldsymbol{\Psi}^s$ form an orthonormal basis in which the displacement vector $\boldsymbol{U}^s$ is searched. These basis vectors are referred to as the modes of the substructure. The computation of projection matrices is explained in section 4.1.

Inserting this relation (eq. (9)) into eq. (8) and applying a Galerkin projection leads to the reduced order model

$$\sum_{s=1}^{n_s} \left(\boldsymbol{\Psi}^{sT} \boldsymbol{R}^s(\boldsymbol{\Psi}^s \boldsymbol{U}^s_{\mathrm{red}}) + \boldsymbol{\Psi}^{sT} \boldsymbol{K}_c^s \boldsymbol{\Psi}^s \boldsymbol{U}^s_{\mathrm{red}} \right) = \sum_{s=1}^{n_s} \boldsymbol{\Psi}^{sT} \boldsymbol{P}^s(\boldsymbol{\Psi}^s \boldsymbol{U}^s_{\mathrm{red}}). \tag{10}$$

This nonlinear reduced system is typically solved with the Newton-Raphson method. For the special case of linear mechanics it reduces further to

$$\sum_{s=1}^{n_s} \boldsymbol{\Psi}^{sT} \boldsymbol{K}^s \boldsymbol{\Psi}^s \boldsymbol{U}^s_{\mathrm{red}} + \boldsymbol{\Psi}^{sT} \boldsymbol{K}_c^s \boldsymbol{\Psi}^s \boldsymbol{U}^s_{\mathrm{red}} = \sum_{s=1}^{n_s} \boldsymbol{\Psi}^{sT} \boldsymbol{P}^s, \tag{11}$$

where the residual vector R^s is replaced by the product of a stiffness matrix and a displacement vector $\boldsymbol{K}^s \boldsymbol{U}^s$. With Dirichlet boundary conditions this system of equations can be solved.

3 MODEL ORDER REDUCTION FOR ANISOTROPIC MATERIALS

In this article, the modules are made of fiber-reinforced materials, and therefore behave transversely isotropic. The fiber orientation of each module is not known before the assembly of the global system and shall be chosen arbitrarily. The mechanical behavior of a substructure depends on the chosen fiber direction, which can be expressed with the fiber angle α. Therefore, the projection matrix $\boldsymbol{\Psi}^s$ and the stiffness matrix $\boldsymbol{K}^s$ or force vector $\boldsymbol{R}^s$ depend on the fiber angle parameter α. For the linear case this leads to the parameter dependent reduced order model

$$\sum_{s=1}^{n_s} (\boldsymbol{\Psi}^s(\alpha))^T \boldsymbol{K}^s(\alpha) \boldsymbol{\Psi}^s(\alpha) \boldsymbol{U}^s_{\mathrm{red}} + (\boldsymbol{\Psi}^s(\alpha))^T \boldsymbol{K}_c^s(\alpha) \boldsymbol{\Psi}^s(\alpha) \boldsymbol{U}^s_{\mathrm{red}} = \sum_{s=1}^{n_s} (\boldsymbol{\Psi}^s(\alpha))^T \boldsymbol{P}^s. \tag{12}$$

To avoid expensive precomputations for every new value of the parameter α the parameter dependent matrices $\boldsymbol{\Psi}^s(\alpha)$ and $\boldsymbol{K}^s(\alpha)$ have to be interpolated. The projection matrices are interpolated on the tangent space of a Grassmann manifold, with the method first introduced in [2], and the stiffness matrices are interpolated with a method based on singular value decomposition.

3.1 Transverse isotropic material model

The material model used in this work is the transverse isotropic model from Reese et al. [16]. To account for the anisotropy a structural tensor is defined

$$\boldsymbol{M} \coloneqq \boldsymbol{n} \otimes \boldsymbol{n}, \tag{13}$$

where $\boldsymbol{n}$ is the normal vector pointing into the fiber direction. The Helmholtz free energy consists then of an isotropic and an anisotropic part

$$\Psi = \Psi(\boldsymbol{C}, \boldsymbol{M}) = \Psi_{\text{iso}}(\boldsymbol{C}) + \Psi_{\text{ani}}(\boldsymbol{C}, \boldsymbol{M}), \tag{14}$$

where the isotropic part only depends on the right Cauchy-Green strain tensor $\boldsymbol{C}$ and the anisotropic part additionally depends on the structural tensor $\boldsymbol{M}$. The material model is formulated in terms of the invariants of the right Cauchy-Green tensor

$$I_1 = \text{tr}(\boldsymbol{C}), \quad I_2 = \frac{1}{2}(I_1^2 - \text{tr}(\boldsymbol{C}^2)), \quad I_3 = \det(\boldsymbol{C}), \tag{15}$$

and two additional invariants depending on the structural tensors $\boldsymbol{M}$

$$I_4 = \boldsymbol{C} : \boldsymbol{M}, \quad I_5 = \boldsymbol{C}^2 : \boldsymbol{M}. \tag{16}$$

The parts of the Helmholtz free energy are

$$\Psi_{\text{iso}} = k_1^{\text{iso}}(I_1 - 3)^2 + k_2^{\text{iso}}(I_2 - 3 - 2(I_1 - 3)) \tag{17}$$

$$\Psi_{\text{ani}} = k_3^{\text{ani}}(I_4 - 1)^2 + k_4^{\text{ani}}(I_5 - 1 - 4(I_4 - 1)) + k_5^{\text{coup}}(I_1 - 3)(I_4 - 1). \tag{18}$$

Since this material model is linear the second Piola Kirchhoff stress is computed with

$$\boldsymbol{S} = \frac{\partial \Psi}{\partial \boldsymbol{E}} = \mathcal{C} : \boldsymbol{E} = (\mathcal{C}_{\text{iso}} + \mathcal{C}_{\text{ani}}) : \boldsymbol{E}, \tag{19}$$

where $\boldsymbol{E}$ is the Green-Lagrange strain tensor. The elasticity tensor consists of an isotropic and an anisotropic part that read

$$\mathcal{C}_{\text{iso}} = (8k_1^{\text{iso}} + 4k_2^{\text{iso}})\boldsymbol{I} \otimes \boldsymbol{I} - 4k_1^{\text{iso}} I, \tag{20}$$

$$\mathcal{C}_{\text{ani}} = 8k_3^{\text{ani}}\boldsymbol{M} \otimes \boldsymbol{M} + 4k_4^{\text{ani}}\mathcal{A} + 4k_5^{\text{coup}}(\boldsymbol{I} \otimes \boldsymbol{M} + \boldsymbol{M} \otimes \boldsymbol{I}), \tag{21}$$

where I is the fourth order identity tensor and $\mathcal{A}$ is a fourth order tensor with the coefficients

$$A_{ijkl} = \frac{1}{2}(\delta_{jk}M_{il} + \delta_{ik}M_{jl} + \delta_{il}M_{jk} + \delta_{jl}M_{ik}). \tag{22}$$

3.2 Interpolation on Grassmann manifolds

Two obtain a projection matrix $\bar{\boldsymbol{\Psi}}$ for a target parameter $\bar{\alpha}$ we interpolate on the geodesic line on the Grassmann manifold between neighboring projection matrices. An $n \times m$-dimensional POD-base $\boldsymbol{\Psi}$ non uniquely defines a point $\mathcal{Y}$ in the Grassmann manifold $\mathcal{G}(m,n)$. All projection matrices have the same number of modes and are on the same Grassmann manifold.

To illustrate the interpolation scheme, we consider two points $\mathcal{Y}_0$ and $\mathcal{Y}_1$ represented by the matrices $\boldsymbol{\Psi}_0$ and $\boldsymbol{\Psi}_1$ with their corresponding parameters α_1 and α_2. The second point is mapped into the tangent

space $\mathcal{T}_{\mathcal{Y}_0}$ of the origin point $\mathcal{Y}_0$ by a logarithmic mapping $\mathcal{X}_1 = \mathrm{Log}_{\mathcal{Y}_0}(\mathcal{Y}_1)$. For Grassmann manifolds this logarithmic mapping is defined as

$$\begin{aligned} \boldsymbol{\Psi}_1(\boldsymbol{\Psi}_0^T\boldsymbol{\Psi}_1)^{-1} - \boldsymbol{\Psi}_0 &= \boldsymbol{W}_1\boldsymbol{\Lambda}_1\boldsymbol{V}_1 \qquad \text{(thin SVD)} \\ \boldsymbol{\Gamma}_1 &= \boldsymbol{W}_1 \arctan(\boldsymbol{\Lambda}_1)\boldsymbol{V}_1 \end{aligned} \tag{23}$$

On this tangent space the matrices can be interpolated with any interpolation method. For this interpolation between two points a linear interpolation is used

$$\bar{\boldsymbol{\Gamma}} = \frac{\bar{\alpha} - \alpha_0}{\alpha_1 - \alpha_0}\boldsymbol{\Gamma}, \tag{24}$$

where $\bar{\boldsymbol{\Gamma}}$ represents the interpolated point $\bar{\mathcal{X}}$ on the tangent space. This point is mapped back to the Grassmann manifold with an exponential mapping $\bar{\mathcal{Y}} = \mathrm{Exp}_{\mathcal{Y}_0}(\bar{\mathcal{X}})$. The exponential mapping is defined as

$$\begin{aligned} \bar{\boldsymbol{\Gamma}} &= \bar{\boldsymbol{W}}\bar{\boldsymbol{\Lambda}}\bar{\boldsymbol{V}} \qquad \text{(thin SVD)} \\ \bar{\boldsymbol{\Psi}} &= \boldsymbol{\Psi}_0\bar{\boldsymbol{V}}\cos(\bar{\boldsymbol{\Lambda}}) + \bar{\boldsymbol{U}}\sin(\bar{\boldsymbol{\Lambda}}), \end{aligned} \tag{25}$$

where $\bar{\boldsymbol{\Psi}}$ is the interpolated projection matrix for the parameter $\bar{\alpha}$.

3.3 Higher order interpolation of matrices

In our method, it is required to accurately interpolate between stiffness matrices and points on the tangent space of the Grassmann manifold. The singular value decomposition enables the reduction of matrix interpolation to a sum of one-dimensional interpolations. For the one-dimensional interpolations, common techniques like cubic spline interpolation can be used. For that, all matrices are converted to a column vector and written into a matrix, which is then multiplicatively split with a SVD

$$\boldsymbol{A} = [\boldsymbol{k}_1, \boldsymbol{k}_2, \ldots, \boldsymbol{k}_n] = \boldsymbol{W}\boldsymbol{\Lambda}\boldsymbol{V} \qquad \text{(thin SVD)}. \tag{26}$$

Since the rows in $\boldsymbol{A}$ correspond to the parameter α the interpolation can be performed in each mode of $\boldsymbol{V}$. For a target parameter $\bar{\alpha}$ this interpolation in $\boldsymbol{V}$ leads to a interpolated vector $\bar{\boldsymbol{v}}$. The interpolated matrix can then be obtained by multiplying $\bar{\boldsymbol{v}}$ with $\boldsymbol{\Lambda}$ and $\boldsymbol{W}$

$$\bar{\boldsymbol{k}} = \boldsymbol{W}\boldsymbol{\Lambda}\bar{\boldsymbol{v}} \tag{27}$$

and reshaping the resulting vector $\bar{\boldsymbol{k}}$ to the matrix format. For the interpolation of stiffness matrices, this method has the advantage that the size of the data is compressed. Instead of all precomputed stiffness matrices only the truncated SVD matrices $\boldsymbol{W}$, $\boldsymbol{\Lambda}$, and $\boldsymbol{V}$ have to be saved.

4 NUMERICAL EXAMPLES

4.1 Precomputations

The projection matrices of each substructure are computed with the method of snapshots (cf. [6]). In this method displacement vectors of a module are collected as columns of the snapshot-matrix and decomposed into three matrices by a singular value decomposition

$$\boldsymbol{S}_{\text{Snap}} = [\boldsymbol{u}_1, \boldsymbol{u}_2, \ldots, \boldsymbol{u}_k] = \boldsymbol{\Phi}\boldsymbol{\Lambda}\boldsymbol{\Upsilon} \qquad \text{(SVD)}. \tag{28}$$

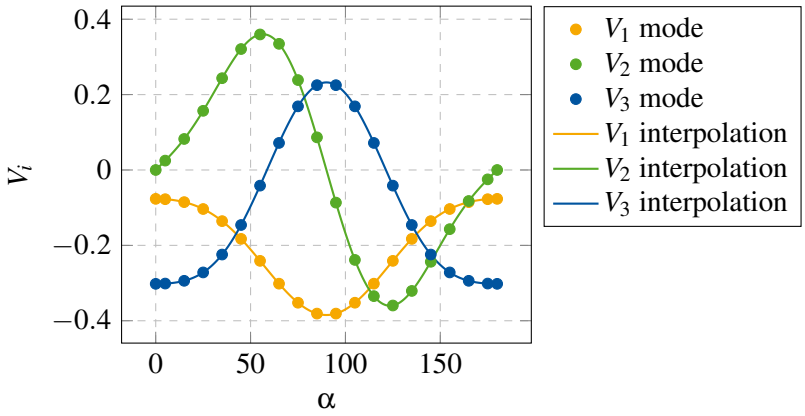

Figure 1: Plot of the first three left modes of stiffness matrices over the fiber angle α. The points are the values in the mode vector and the lines are their interpolation with cubic splines.

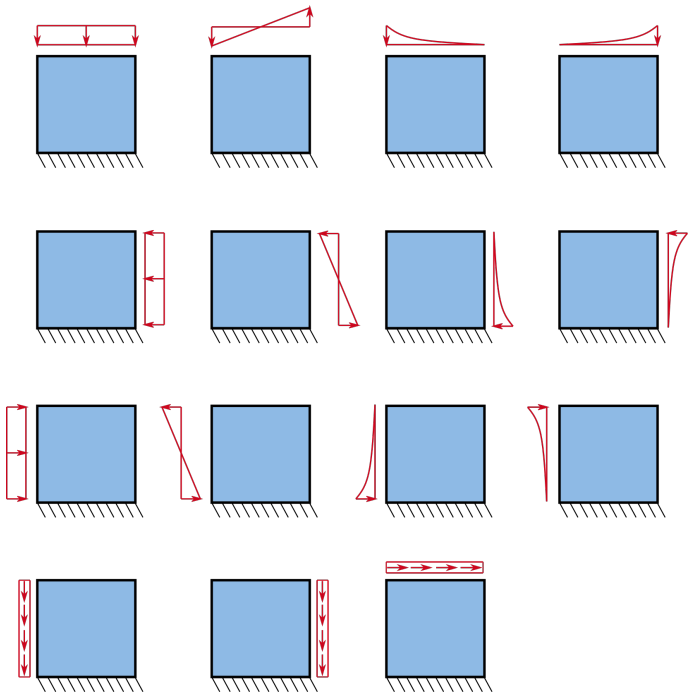

Figure 2: Illustration of boundary conditions for the snapshot computations of the square module. The same snapshots are computed for all four sides of the Dirichlet boundary condition.

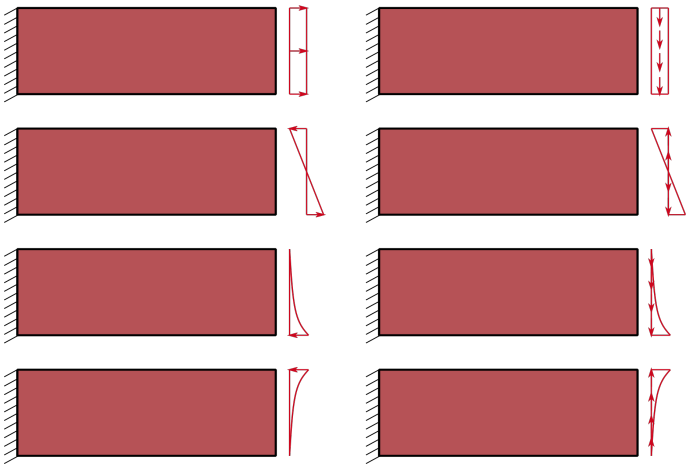

Figure 3: Illustration of boundary conditions for the snapshot computations of the rectangular module. The same snapshots are computed for the Dirichlet boundary conditions on the opposite side.

The projection matrix is obtained by taking only the first m columns of the matrix $\mathbf{\Phi}$ into account

$$\mathbf{\Psi} = [\Phi_1, \Phi_2, \ldots, \Phi_m]. \tag{29}$$

To compute projection matrices that work for the modular model order reduction the snapshots have to be representative of the mechanical behavior of the module.

In this work, two exemplary modules are considered. The first module is a square discretized with 7442 elements, and the second module is a rectangle with 12322 elements. For both modules, the projection matrices have to be computed for different values of the fiber angle α. For the square, the projection matrices are computed at angles between 0° and 90° in steps of 10°. The projection matrices of the rectangular module are computed in the range between 0° and 180° to account for coordinate transformations when the module is rotated. The snapshots of each module contain snapshots that are generated with two methods. In the first method, snapshots are computed by representative load cases and clamping boundary conditions on one side of the module. This load cases are illustrated in fig. 2 for the square, and fig. 3 for the rectangular module. The load cases of the square are computed for clamping of each side of the module in the same way as it is illustrated in fig. 2 for clamping of the bottom side. For the precomputations of the rectangle, the load cases shown in fig. 3 are computed for clamp boundary conditions on the left and on the right side.

Additionally, snapshots for contact surface deformation are needed. First, all degrees of freedom on possible interfaces are fixed, then a unit displacement is applied to each of the degrees of freedom separately. The resulting displacement vectors are stored as columns in a matrix analogously to the snapshot matrix. The dominant POD modes of this matrix are used as snapshots for the projection matrix.

Furthermore, snapshots with rigid body deformations like rotation and translation are needed.

The resulting projection matrix of the square has 52 modes, and the projection matrix of the rectangle has 40 modes. This relatively large number of modes is necessary to use the modules with different contact- and loading conditions. The mode-matrix for the interpolation of the stiffness matrices contains five modes for both modules.

4.2 Example 1: Uniform fiber orientation

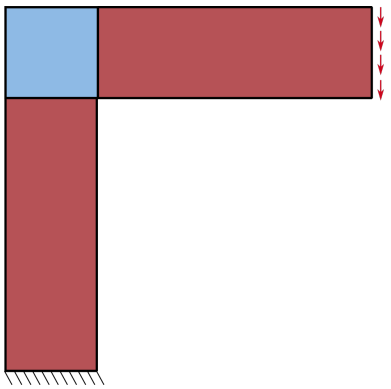

Figure 4: Sketch of the modular system for the first numerical example. The fiber direction in each module is the same. The red arrows illustrate the Neumann boundary conditions. The degrees of freedom at the bottom are fixed with Dirichlet boundary conditions.

In the first example, the quality of the solution with the reduced-order model is analyzed over the whole parameter range. The geometry of the system with its Dirichlet- and Neumann boundary conditions, is shown in fig. 4. The structure is made of two rectangular and one square module, where one of the rectangles is rotated by 90°. The fiber orientation in each module is the same. For each fiber direction, three solutions are computed. The first solution is an unreduced reference solution where the stiffness matrices of each module are computed normally. For the other two solutions, the stiffness matrices are interpolated with the method described in section 3.3. The second solution is unreduced, and the third solution is reduced.

The norms to quantify the error are

$$e_u = \frac{\| \boldsymbol{u}_{\mathrm{MOR}} - \boldsymbol{u}_{\mathrm{ref}} \|}{\| \boldsymbol{u}_{\mathrm{ref}} \|}, \quad \text{and} \quad e_\sigma = \frac{\| \boldsymbol{\sigma}_{\mathrm{MOR}} - \boldsymbol{\sigma}_{\mathrm{ref}} \|}{\| \boldsymbol{\sigma}_{\mathrm{ref}} \|}, \tag{30}$$

where e_u is the displacement error and e_σ is the stress error norm. In fig. 5 the errors are plotted over the fiber orientation angle α.

The displacement errors of the reduced solution range between $1.7\ 10^{-4}$ and $3.54\ 10^{-3}$. The stress errors of the reduced solution are higher and range between $3.9\ 10^{-2}$ and $9.1\ 10^{-2}$. The displacement error grows with increasing fiber angle α, while the stress error has a peak for small values of α and for large values of α. For small angles, the stiffness in the horizontal rectangle is maximum, and for large angles the stiffness in the vertical rectangle is maximum. This suggests, that the MOR of the rectangle for high stiffnesses performs slightly worse. Displacement errors in the vertical rectangle lead to displacement errors in the horizontal rectangle, while displacement errors in the horizontal rectangle do not influence the vertical rectangle. This leads to the larger displacement errors for higher values of the fiber angle α.

4.3 Example 2: Random fiber orientation

The second example consists of 24 modules, where a random fiber direction is assigned to every module. The geometry of the system with its Dirichlet- and Neumann boundary conditions, is shown in

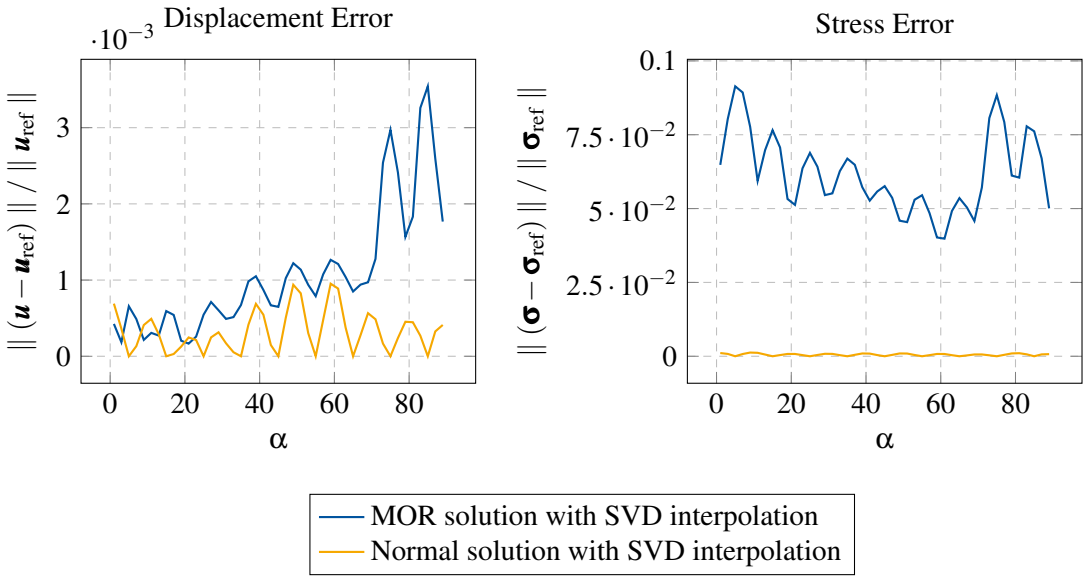

Figure 5: Displacement and stress error over the fiber angle α for the first numerical example with uniform fiber orientation.

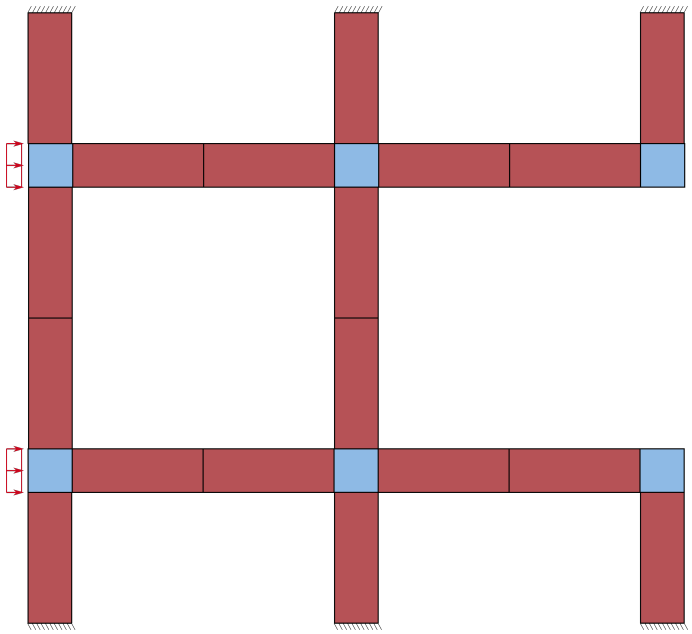

Figure 6: Sketch of the modular system for the second numerical example. The fiber direction in each module is random. Dirichlet boundary conditions are applied on all degrees at the top and the bottom of the structure. The red arrows illustrate the Neumann boundary conditions.

fig. 6. The random fiber orientation requires interpolation of the projection matrix as well as the stiffness matrix of every module. The system has originally 266448 degrees of freedom and is reduced to 1032 degrees of freedom. The unreduced computation took 251.9 and the reduced computation 15.2 seconds. The speed-up factor $f = t_{\text{normal}}/t_{\text{MOR}}$ is 16.57. The interpolation of stiffness matrices and projection matrices for the reduced computation took 9.4 seconds. This time includes the projection of all stiffness matrices into the reduced space. The assembly of the system of equations took 5.45 and the solution 0.35 seconds. In the assembly process also the contact terms and Dirichlet boundary conditions are projected into the reduced space. The computational time can be decreased by a more efficient implementation in a low-level language like FORTRAN or C.

The displacement and stress errors norms defined in eq. (30) are $e_u = 0.0012$ and $e_\sigma = 0.067$. As in fig. 5, the stress error is one magnitude larger than the displacement error. The approximation of the stress field is still accurate. These results are analogous to the results in fig. 5.

In fig. 7 the contour plots of the von Mises stress and the von Mises stress error norm $e_{\sigma_v} = (\mid \sigma_{v,\text{MOR}} - \sigma_{v,\text{ref}} \mid)/(\mid \sigma_{v,\text{ref}} \mid)$ are shown. It can be seen, that the qualitative differences in the contour plots of both solutions are subtle. Large errors above 0.1 concentrate on the connection of four rectangles with one square and are mostly at positions with small von Mises stress. Areas with high von Mises stress tend to have a small error. The contour plots show that the reduced modular computation gives reasonable stress results, even though global stress error norms are higher than the displacement errors.

The results show that the modules can be used in a flexible way. The square module is used with two, three, and four adjacent modules, where always the same projection matrices are used to reduce the module.

5 CONCLUSION

In this work, a model order reduction technique was presented, where global structures are assembled from locally reduced modules. Furthermore, parameter dependencies of the reduced system coming from anisotropic material behavior were analyzed. The adaption of the projection matrices for different fiber directions was done by interpolation on a tangent space of the Grassmann manifold. With a singular value decomposition, the interpolation of stiffness matrices could be reduced to a sum of one-dimensional cubic spline interpolations. In the first numerical example, it was shown that the adaption of the reduced system gives reasonable results over the whole parameter range. The second example showed, that the method can also be applied to more complex structures and achieves a significant speed-up compared to the unreduced solution.

In the future, a set of modules has to be developed, that allows for the computation of complex real-world structures. Furthermore, the method has to be applied to nonlinear problems. The direct empirical interpolation method (DEIM) can be used to approximate the nonlinear term and parameter-dependent linear stiffness matrices.

6 ACKNOWLEDGEMENTS

Funding granted by the subproject A01 of the transregional Collaborative Research Center 280 with the project number 417002380 is gratefully acknowledged. Additionally, the authors acknowledge the funding of the project ”Model order reduction in space and parameter dimension - towards damage based modeling of polymorphic uncertainty in the context of robustness and reliability”, project number 312911604, from the priority program SPP 1886.

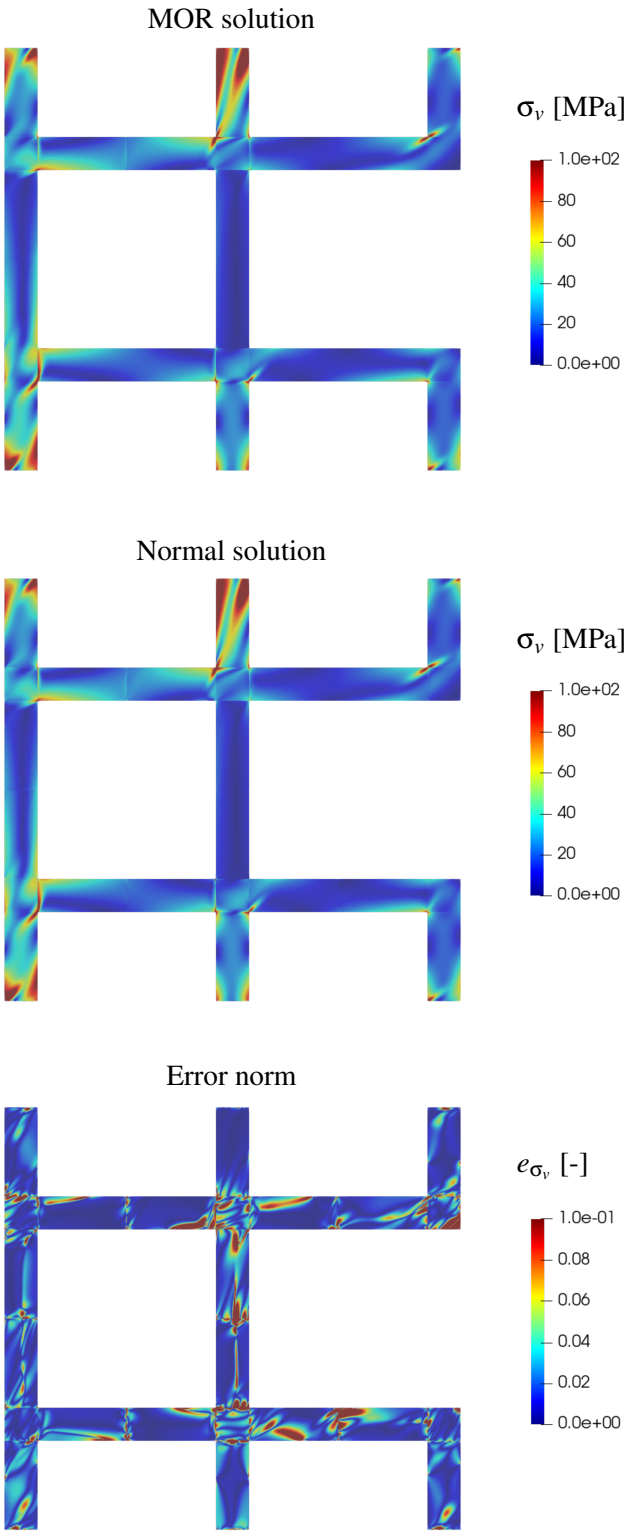

Figure 7: Contour plots of von Mises stresses for the unreduced (top) and reduced (middle) solution. The contour plot at the bottom shows the error norm of the von Mises stresses.

REFERENCES

[1] D. Amsallem, J. Cortial, K. Carlberg, and C. Farhat. A method for interpolating on manifolds structural dynamics reduced-order models. *International journal for numerical methods in engineering*, 80(9):1241–1258, 2009.

[2] D. Amsallem and C. Farhat. Interpolation method for adapting reduced-order models and application to aeroelasticity. *AIAA journal*, 46(7):1803–1813, 2008.

[3] A. C. Antoulas. An overview of approximation methods for large-scale dynamical systems. *Annual reviews in Control*, 29(2):181–190, 2005.

[4] P. Benner, S. Gugercin, and K. Willcox. A survey of projection-based model reduction methods for parametric dynamical systems. *SIAM review*, 57(4):483–531, 2015.

[5] B. Besselink, U. Tabak, A. Lutowska, N. Van de Wouw, H. Nijmeijer, D. J. Rixen, M. Hochstenbach, and W. Schilders. A comparison of model reduction techniques from structural dynamics, numerical mathematics and systems and control. *Journal of Sound and Vibration*, 332(19):4403–4422, 2013.

[6] K. S. Breuer and L. Sirovich. The use of the karhunen-loeve procedure for the calculation of linear eigenfunctions. *Journal of Computational Physics*, 96(2):277–296, 1991.

[7] D. de Klerk, D. J. Rixen, and S. Voormeeren. General framework for dynamic substructuring: history, review and classification of techniques. *AIAA journal*, 46(5):1169–1181, 2008.

[8] O. Friderikos, E. Baranger, M. Olive, and D. Neron. On the stability of pod basis interpolation on grassmann manifolds for parametric model order reduction. *Computational Mechanics*, pages 1–24, 2022.

[9] S.-K. Hong, B. I. Epureanu, M. P. Castanier, and D. J. Gorsich. Parametric reduced-order models for predicting the vibration response of complex structures with component damage and uncertainties. *Journal of sound and vibration*, 330(6):1091–1110, 2011.

[10] S. Kastian, D. Moser, L. Grasedyck, and S. Reese. A two-stage surrogate model for neo-hookean problems based on adaptive proper orthogonal decomposition and hierarchical tensor approximation. *Computer Methods in Applied Mechanics and Engineering*, 372:113368, 2020.

[11] G. Kerschen, J.-c. Golinval, A. F. Vakakis, and L. A. Bergman. The method of proper orthogonal decomposition for dynamical characterization and order reduction of mechanical systems: an overview. *Nonlinear dynamics*, 41(1):147–169, 2005.

[12] X. Pennec, P. Fillard, and N. Ayache. A riemannian framework for tensor computing. *International Journal of computer vision*, 66(1):41–66, 2006.

[13] A. Popp and P. Wriggers. *Contact modeling for solids and particles*, volume 585. Springer, 2018.

[14] A. Radermacher and S. Reese. Model reduction in elastoplasticity: proper orthogonal decomposition combined with adaptive sub-structuring. *Computational Mechanics*, 54(3):677–687, 2014.

[15] A. Radermacher and S. Reese. Pod-based model reduction with empirical interpolation applied to nonlinear elasticity. *International Journal for Numerical Methods in Engineering*, 107(6):477–495, 2016.

[16] S. Reese, T. Raible, and P. Wriggers. Finite element modelling of orthotropic material behaviour in pneumatic membranes. *International journal of solids and structures*, 38(52):9525–9544, 2001.

[17] L. Zhou, J.-W. Simon, and S. Reese. Proper orthogonal decomposition for substructures in nonlinear finite element analysis: coupling by means of tied contact. *Archive of Applied Mechanics*, 88(11):1975–2001, 2018.